UC Berkeley
UC Berkeley Previously Published Works

Title

A scalable solid-state nanoporous network with atomic-level interaction design for carbon dioxide capture

Permalink

https://escholarship.org/uc/item/278276xt

Journal

Science Advances, 8(31)

ISSN

2375-2548

Authors

Mao, Haiyan
Tang, Jing
Day, Gregory S
et al.

Publication Date

2022-08-05

DOI

10.1126/sciadv.abo6849

Peer reviewed

MATERIALS SCIENCE

A scalable solid-state nanoporous network with atomic-level interaction design for carbon dioxide capture

Haiyan Mao[1]†, Jing Tang[2,3]†, Gregory S. Day[4], Yucan Peng[2], Haoze Wang[5], Xin Xiao[2], Yufei Yang[2], Yuanwen Jiang[6], Shuo Chen[1], David M. Halat[1,7], Alicia Lund[1]‡, Xudong Lv[5], Wenbo Zhang[2], Chongqing Yang[8], Zhou Lin[5], Hong-Cai Zhou[4], Alexander Pines[5], Yi Cui[2,3]*, Jeffrey A. Reimer[1,7]*

Carbon capture and sequestration reduces carbon dioxide emissions and is critical in accomplishing carbon neutrality targets. Here, we demonstrate new sustainable, solid-state, polyamine-appended, cyanuric acid–stabilized melamine nanoporous networks (MNNs) via dynamic combinatorial chemistry (DCC) at the kilogram scale toward effective and high-capacity carbon dioxide capture. Polyamine-appended MNNs reaction mechanisms with carbon dioxide were elucidated with double-level DCC where two-dimensional heteronuclear chemical shift correlation nuclear magnetic resonance spectroscopy was performed to demonstrate the interatomic interactions. We distinguished ammonium carbamate pairs and a mix of ammonium carbamate and carbamic acid during carbon dioxide chemisorption. The coordination of polyamine and cyanuric acid modification endows MNNs with high adsorption capacity (1.82 millimoles per gram at 1 bar), fast adsorption time (less than 1 minute), low price, and extraordinary stability to cycling by flue gas. This work creates a general industrialization method toward carbon dioxide capture via DCC atomic-level design strategies.

INTRODUCTION

The increasing concentration of greenhouse gases in the atmosphere is a critical environmental concern (1, 2). In 2021, the U.S. government pledged to reach carbon neutrality before 2050, with carbon neutrality referring to the achievement of net zero carbon dioxide emissions (3). In 2018, carbon dioxide emissions from the combustion of fossil fuels were about 75% of the total U.S. anthropogenic greenhouse emissions (4). Carbon capture, utilization, and sequestration (CCUS) comprises essential requirements to achieve carbon neutrality (5, 6). However, there are many challenges toward making CCUS a reality, notably capturing costs and energy consumption (5). The U.S. Department of Energy (DOE) has previously announced projects with a total value of $3.18 billion to boost advanced and commercially scalable technologies with CCUS to reach an ambitious flue gas emission CO_2 capture efficiency target of 90% (7, 8). Therefore, extensive efforts have been made to develop advanced materials that simultaneously reduce CO_2 capture costs and energy consumption while being greener, cheaper, and more scalable than previous CCUS technologies (5).

Aqueous polyamines generate dynamic libraries of ligands for spontaneous CO_2 fixation with the advantage of rapid and reversible reaction with CO_2, as well as low solvent cost (8). Aqueous polyamines have significant limitations, however, including decomposition of volatile amines, high energy consumption during solvent regeneration,

equipment corrosion, and emissions that can be problematic for both environmental and human health (9). To overcome these limitations, amine-functionalized adsorbents have been proposed as an alternative to aqueous polyamines, having noncorrosive properties while still maintaining the high chemical selectivity and stability of the amine reaction with CO_2. Adsorbents such as amine-functionalized metal-organic frameworks (MOFs) could usher in a new era for CCUS due to their high adsorption capacity and cooperative CO_2 adsorption (9, 10). Nevertheless, boosting performance in capacities, chemical stability, and scalability of MOFs requires atomic-level understanding and further exploration of material options. Compared to MOFs, polymer-based porous adsorbents can be synthesized to be metal-free, sustainable, and derived from cheap raw materials, all of which are essential for mass production (11, 12).

At the kilogram scale, we demonstrate the new sustainable solid-state, polyamine-appended, cyanuric acid–stabilized melamine nanoporous networks (MNNs) via dynamic combinatorial chemistry (DCC) to achieve effective, scalable, recyclable, and high-capacity CO_2 capture. MNNs, synthesized from commercial melamine and paraformaldehyde, are promising for reversible CO_2 capture owing to the intriguing advantages of their robust flake-like structures, high surface areas, tunable surface chemistries, and industrial-scale capture capabilities. The nature of the chemisorption mechanism at the atomic level is essential for the design of polyamine-appended networks with high CO_2 capacity. A quantitative assessment of the local bonding environment and the mechanism at the atomic level for the adsorption of CO_2 with these networks is required to further the design of MNNs with high CO_2 adsorption capacity for CCUS.

Solid-state nuclear magnetic resonance (NMR) provides information about an atom-by-atom basis to reveal the chemical structure and dynamics of solid porous materials (13). Because NMR signals are derived from the magnetism of atomic nuclei (especially the magnetic moment and angular momentum of nuclear spins), NMR is a spectroscopic technique in which a specific signal can be detected from each atom in a molecule (13). The frequency peaks are assigned to individual atoms, utterly different from other frequency

[1]Department of Chemical and Biomolecular Engineering, University of California, Berkeley, Berkeley, CA 94720, USA. [2]Department of Materials Science and Engineering, Stanford University, Stanford, CA 94305, USA. [3]Stanford Institute for Materials and Energy Sciences, SLAC National Accelerator Laboratory, 2575 Sand Hill Road, Menlo Park, CA 94025, USA. [4]Department of Chemistry, Texas A&M University, College Station, TX 77843, USA. [5]Department of Chemistry, University of California, Berkeley, Berkeley, CA 94720, USA. [6]Department of Chemical Engineering, Stanford University, Stanford, CA 94305, USA. [7]Materials Sciences Division, Lawrence Berkeley Laboratory, Berkeley, CA 94720, USA. [8]The Molecular Foundry, Lawrence Berkeley National Laboratory, Berkeley, CA 94720, USA.
*Corresponding author. Email: yicui@stanford.edu (Y.C.); reimer@berkeley.edu (J.A.R.)
†These authors contributed equally to this work.
‡Present address: Covalent Metrology, 921 Thompson Place, Sunnyvale, CA 94085, USA.

peaks (e.g., infrared and Raman spectra). As a result, multidimensional NMR spectroscopy can be tailored according to a given chemical system to provide precise information about the interaction between atoms that cannot be gained in other structural technologies. For example, in the two-dimensional (2D) heteronuclear correlation (HETCOR) measurement, the correlation is mediated by either through-bond J coupling or through-space dipolar coupling [13]. In addition, NMR spectroscopy has identified local interatomic interactions in hybrid composites using quantitative measurement techniques [14]. High-resolution methods, including ^{13}C cross-polarization magic-angle spinning (CP-MAS) NMR and 2D HETCOR spectroscopy, can provide critical mechanistic and dynamic insights into the local environment, short-range structure, and interatomic interaction mechanism between CO_2 molecules and MOFs [14, 15].

DCC is one candidate for creating such a library wherein all constituents are in equilibrium under thermodynamic control [16], and the library members interconvert through reversible chemical processes involving covalent bonds or noncovalent interactions. Research on using DCC to craft binding sites for CO_2 on a neutral target is currently scarce [8]. MNNs present a diverse array of materials, and thus, a targeted, systematic search for a library of materials for carbon capture is important. In this study, we develop new long-term, polyamine-appended, cyanuric acid–stabilized MNNs via DCC at the kilogram scale for effective, scalable, recyclable, and high-performance CO_2 capture.

Here, we use DCC to design interconverting species of amine [e.g., diethylenetriamine (DETA)]–appended MNNs for CO_2 capture. We interrogate the cyanuric acid–modified DETA-appended MNNs (MNNs^{Cya} ⊃ DETA) structure by multinuclear NMR spectroscopy and density functional theory (DFT) calculations, uncovering the origin of the stability of chemisorbed CO_2 during adsorption-desorption cycles. To further demonstrate the applicability of MNNs^{Cya} ⊃ DETA for CCUS, we measured adsorption time scales, cycling stability, and regeneration energy of the networks. Our work establishes that these systems exhibit scalable and affordable carbon capture properties and affirms the strategy of DCC-induced solid-state porous network design as a sustainable method for long-term gas storage.

RESULTS

MNN modification and characterization

To enhance the CO_2 chemisorption and its adsorption-desorption stability, we synthesized MNNs^{Cya} ⊃ DETA (Fig. 1, A to D) at a kilogram scale (fig. S1) using a designed scalable setup (Fig. 1E). In this modified network, cyanuric acid was introduced as an MNN dopant during polymerization and used as noncovalent anchor sites for alkylamines to ultimately maintain the CO_2 adsorption capacity and improve chemical stability. The addition of DETA enabled an increase in CO_2 chemisorption capacity. Figure 1F shows typical transmission electron microscopy (TEM) micrographs of the microtomed particles imaged under different magnifications, indicating that micro- and mesopores were developed [17]. The pore size distribution of the networks suggests a mesopore-dominated structure, with a small fraction of micropores, as shown in fig. S2. The TEM result demonstrates an amorphous phase in the microporous and mesoporous structure, which is consistent with the pore size distribution results (fig. S2).

We first sought to determine the structures of modified MNNs before the adsorption of CO_2. We examined the cyanuric acid–modified amine-appended MNNs in detail as a benchmark material via solid-state NMR. Our investigation began with the structure of MNNs^{Cya} (Fig. 1C), which was determined using quantitative ^{13}C MAS NMR spectra by direct excitation (fig. S3). The MNN spectrum presents a sharp peak at 166.5 parts per million (ppm) emanating from the triazine ring of melamine, while the two overlapping broad peaks at around 50.0 ppm arise from the —NH—CH_2—NH— aminal group and the —NH—CH_2—OH terminal hemiaminal group, respectively (fig. S3A). After cyanuric acid dopant incorporation, the signals observed at 150.0 and 40.3 ppm are attributed to triazine ring **C**—O bonds and —NH—CH_2—O—, respectively [18].

We subsequently measured the ^{13}C CP-MAS NMR spectra of DETA, MNNs ⊃ DETA, and MNNs^{Cya} ⊃ DETA via CP from ^{1}H to ^{13}C nuclei with heteronuclear decoupling (fig. S3B). The DETA spectrum exhibits two peaks at 53.6 and 42.7 ppm, attributed to the CH_2 groups from —CH_2—NH—CH_2 and —CH_2—NH_2, respectively. These DETA signals persist in the MNNs ⊃ DETA and MNNs^{Cya} ⊃ DETA spectra, at 53.0 and 42.0 ppm, respectively. Thus, DETA molecules are successfully appended to the networks, presumably by hydrogen bonding during post-synthetic modification.

We performed direct detection of ^{13}C MAS NMR spectra (i.e., without CP) of the MNN series to provide a quantitative spectrum that would assist in identifying the structures of modified MNNs. All spectra were deconvoluted and integrated using the dmfit software [19] (fig. S4) with the spectral simulation parameters (table S1). This analysis provides information about the relative proportion of triazine rings within MNNs and of the triazine rings of cyanurate within MNNs^{Cya}. Through this quantitative ^{13}C NMR spectroscopy, we were able to confirm the structures of MNNs^{Cya}, MNNs ⊃ DETA, and MNNs^{Cya} ⊃ DETA, consistent with the DFT-calculated structures at the TPSS-D3(BJ)/6-31G* level in Q-Chem 5.4 (Fig. 1, A to D) [20]. Cyanuric acid molecules were inserted into the triazine rings within MNNs (N^2,N^4,N^6-trimethyl-1,3,5-triazine-2,4,6-triamine) with a ratio of 1:6, based on the results from the quantitative ^{13}C NMR spectra (fig. S4 and table S1). The positions of the inserted DETA molecules fell at the edges of MNN^{Cya} networks and were bound through two amine groups to the framework —NH— sites by hydrogen bonds with an average N…H distance of 2.12 Å (Fig. 1D). The ^{13}C MAS NMR spectra of MNNs^{Cya} ⊃ DETA as a function of pressure are shown in fig. S5.

Last, ^{15}N CP-MAS NMR experiments were conducted for further structure determination. The ^{15}N NMR spectrum of cyanuric acid–modified MNNs^{Cya} shows a weak resonance at 147.0 ppm (fig. S3C), assigned to the nitrogen within the triazine ring of cyanurate (2,4,6-trimethoxy-1,3,5-triazine), while the ^{15}N signal of the cyanuric acid nitrogen is located at 136.0 ppm. The weak signal within the ^{15}N spectrum of MNNs^{Cya} is due to the low concentration of cyanuric acid [7.5 mole percent (mol %)] in MNNs^{Cya}. The chemical shift difference (11 ppm) between the aforementioned two spectra is probably due to triazine ring currents from MNNs (N^2,N^4,N^6-trimethyl-1,3,5-triazine-2,4,6-triamine) within MNNs^{Cya}, as discussed previously [19]. The ^{15}N spectra of MNNs ⊃ DETA and MNNs^{Cya} ⊃ DETA also confirm that DETA was successfully appended into the networks (fig. S3C). The two distinct peaks of the ^{15}N spectra of MNNs ⊃ DETA and MNNs^{Cya} ⊃ DETA, which appear after DETA postmodification, are located at 30.3 and 20.1 ppm, corresponding to —**N**H— and **N**H_2— within the appended DETA, respectively. The emergence of these two peaks from DETA plays an essential role in reaction with CO_2.
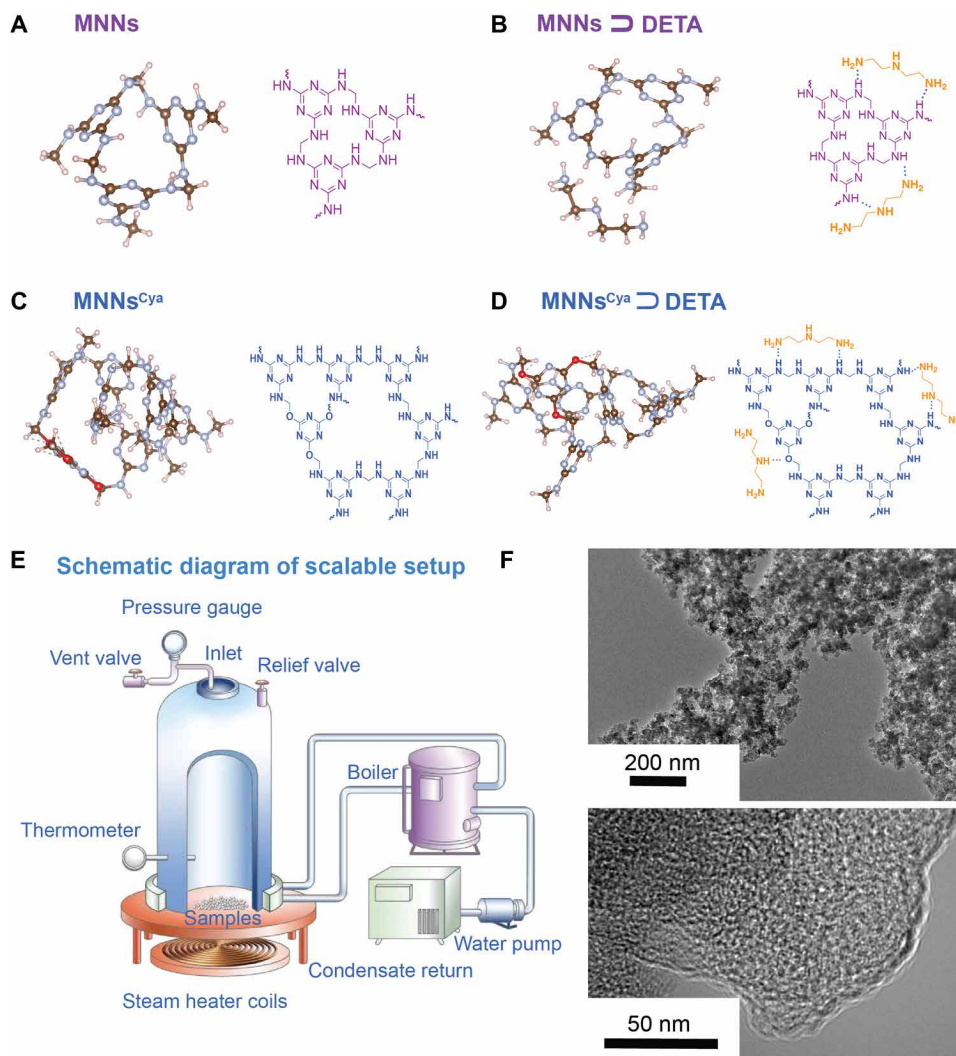
**Fig. 1. Structures of DETA coordination in MNNs.** (**A** to **D**) Structure of MNNs, MNNs ⊃ DETA, MNNs^{Cya}, and MNNs^{Cya} ⊃ DETA. For each subfigure, the left shows a channel of MNN series viewed in the *ab* plane, using the DFT-optimized structures. The right subfigure shows the chemical structure. (**E**) Schematic diagram of the scalable setup. (**F**) TEM of MNNs^{Cya} ⊃ DETA. The structures (A, B, C, and D) were confirmed by quantitative direct excitation ^{13}C NMR spectroscopy and DFT calculations at the TPSS-D3(BJ)/6-31G* level. Brown, silver, pink, and red spheres represent C, N, H, and O atoms, respectively.

CO₂ adsorption properties

We conducted CO_2 adsorption isotherms of MNNs and MNNs^{Cya} ⊃ DETA at room temperature (298 K), shown in Fig. 2A. Both samples have typical Langmuir-type isotherms commonly observed for microporous materials that favor gas adsorption (*21*). Notably, an increase in CO_2 uptake for MNNs^{Cya} ⊃ DETA is observed, relative to the unmodified material, from 0.91 to 1.82 mmol/g at 1 bar, presumably due to the successful incorporation of cyanuric acid and DETA into MNNs. Our results indicate that the DETA and cyanuric acid–modified MNNs have a high affinity and adsorption capacity of CO_2, making them suitable for direct CO_2 capture.

Further solid-state ^{13}C and ^{15}N NMR measurements enabled us to examine the underlying mechanisms for the formation of ammonium carbamate and carbamic acid during CO_2 adsorption. We used a custom-built gas dosing setup to achieve $^{13}CO_2$ adsorption onto network materials with a precise gas flow in a sealed system (fig. S6) (*19*). This system affords the use of commercial MAS rotors

while enabling controlled gas dosing of activated network samples. Here, $^{13}CO_2$ gas dosing was performed at various pressures up to ~1 bar (298 K) using the system pressure gauge that precisely monitored the equilibration of $^{13}CO_2$ adsorption before the acquisition of the ^{13}C MAS NMR spectra. In all measurements, ^{13}C-labeled $^{13}CO_2$ gas could be readily distinguished from unlabeled carbon within the networks owing to its high ^{13}C enrichment level. Starting from bare MNNs, the direct ^{13}C NMR spectra (Fig. 2B) for two scans of $^{13}CO_2$-dosed MNNs display a prominent resonance that corresponds to physisorbed CO_2 at 125.4 ppm. As expected, we also observe a peak at 125.4 ppm, assignable to physisorption of CO_2 in the ^{13}C NMR spectra of $^{13}CO_2$-dosed MNNs^{Cya}, with further signal averaging as compared to $^{13}CO_2$-dosed MNNs. Under these conditions, a second peak at 166.4 ppm is also observed and assigned to the resonance from the triazine ring of the networks (Fig. 2B). The chemical shift of physisorbed CO_2 within MNNs is shifted by −2.3 ppm relative to free gaseous CO_2 at 127.7 ppm at 1 bar (*22*), likely due to the
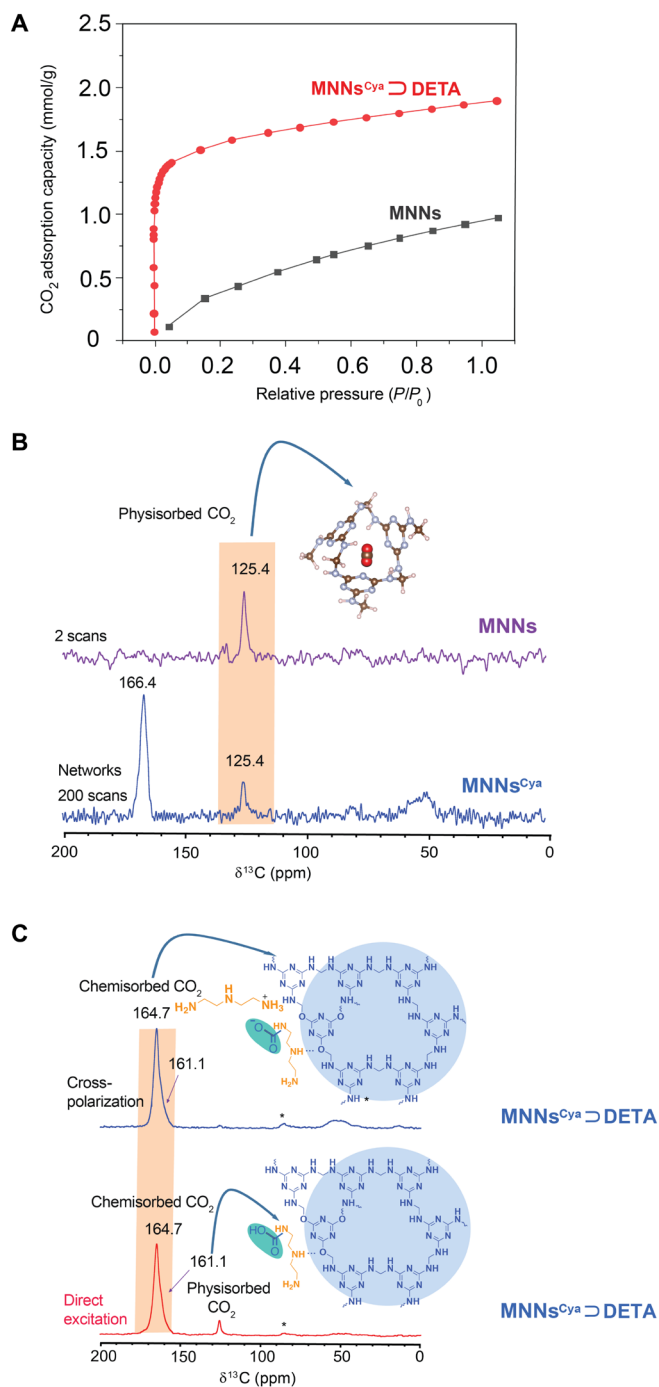
Fig. 2. CO_2 adsorption isotherms and solid-state MAS NMR (16.4 T) spectra of MNNs, MNNs^{Cya}, and MNNs^{Cya} ⊃ DETA with CO_2. (**A**) Adsorption isotherms for CO_2 uptake in MNNs and MNNs^{Cya} ⊃ DETA at 298 K. (**B**) Direct excitation ^{13}C MAS NMR spectra of $^{13}CO_2$-adsorbed MNNs and MNNs^{Cya}. (**C**) Direct excitation and cross-polarized ^{13}C MAS NMR spectra of CO_2-adsorbed MNNs^{Cya} ⊃ DETA. All NMR experiments were performed at room temperature.

shielding effect of the triazine ring currents in the frameworks. A similar result was also previously reported for MOF-274 because of aromatic ring currents arising from the linkers (*22*). Figure 2C and fig. S7 depict the ^{13}C NMR spectra of $^{13}CO_2$-dosed DETA-appended MNNs and MNNs^{Cya} obtained via direct excitation and CP experiments.

The latter experiment allows for the much faster detection of chemisorbed CO_2 by proton CP from the ^1H-rich networks. The direct detection spectra exhibit a peak at 125.4 ppm caused by CO_2 physisorption in the networks.

The distinct peak observed at ~165 ppm, assigned to chemisorbed CO_2, consists of a sharper (164.7 ppm) and a broader (161.1 ppm) component (Fig. 2C). We identify the former chemisorbed species as ammonium carbamate, with the latter being a minor chemisorption product, carbamic acid. The chemical shifts are similar to those previously assigned to ammonium carbamate and carbamic acid (*22*). Quantitative ^{13}C NMR spectra reveal that the overwhelming majority (92%) of adsorbed CO_2 is chemisorbed at 1 bar, and only a small amount (~8%) is physisorbed at this pressure (table S1). Of the chemisorbed species, carbamic acid comprises a minor percentage (20%) of the reaction products, while ammonium (80%) carbamate dominates the chemisorption products (table S1). The spectra of CO_2-adsorbed MNNs^{Cya} ⊃ DETA and MNNs ⊃ DETA are very similar, suggesting similar chemisorbed products (ammonium carbamate and carbamic acid).

Chemisorption mechanism in the context of DCC

DCC allows individual species to interconvert through a reversible bond exchange process that involves either covalent bonds or noncovalent interactions (*23*). Whether covalent or noncovalent, dynamic bonds are crucial to access distinct self-assembled structures that produce the most thermodynamically stable species (*24*). Here, CO_2-derived building blocks are generated via a strategy of combining two reversible covalent bonds (imines and carbamates) and therefore hold enormous potential for CO_2 capture (Fig. 3A). Figure 3 (B and C) detail the five hypothetical structures that may be generated from the N—CO_2 reactions in the MNNs^{Cya} ⊃ DETA, using a double-level dynamic combinatorial system (*25*, *26*). The system comprises first-level carbamation (Fig. 3B) and second-level ion-pairing reactions (Fig. 3C). At the first level, the exposure of CO_2 to MNNs^{Cya} ⊃ DETA leads to the formation of ammonium carbamate and carbamic acid. This occurs through reversible reactions, exchange, and generation of a dynamic system of species (Fig. 3B, eqs. 1 and 2). It has been demonstrated that structural diversity within a dynamic combinatorial system can be expanded by maintaining two communicating exchange processes simultaneously (*27*, *28*). Consequently, in the presence of excess CO_2, a system driven by DCC may display a sequential reaction between or within system members, giving rise to second-level paired structures (Fig. 3C). Depending on the degree of protonation and carbamation, these paired structures may potentially encompass ammonium carbamate chains (Fig. 3C, eq. 3), carbamic acid pairs (Fig. 3C, eq. 4), and mixed carbamate and carbamic acid pairs via Lewis acid sites (Fig. 3C, eq. 5). In particular, the above reversible reactions can eventually revert to the initial reactants under thermodynamic control. From this perspective, if the combinatorial species can bind intermolecularly to induce self-pairing, then this process will lead to self-assembly and strongly contribute to favorable CO_2 adsorption isotherms.

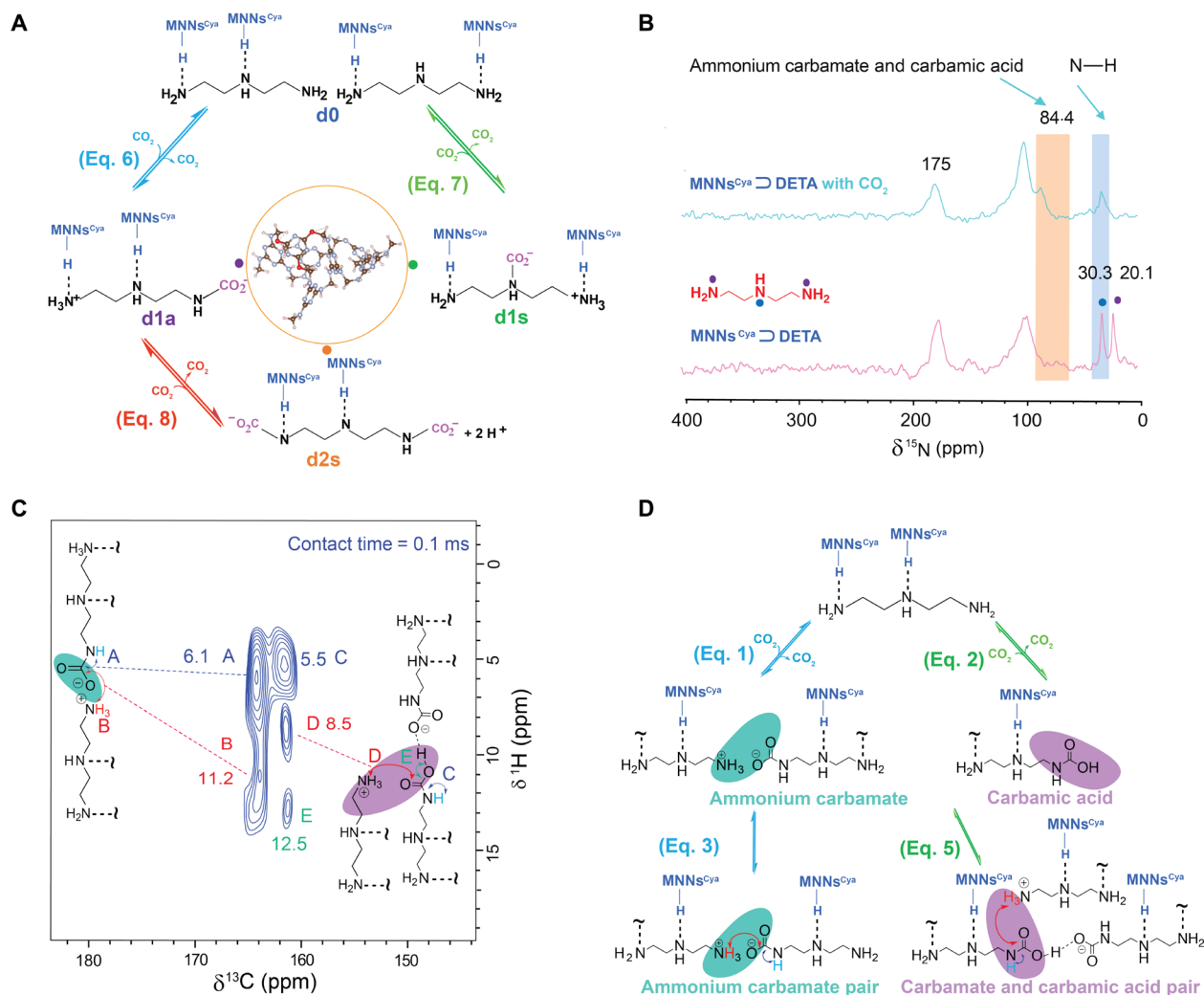**Demonstration of the dynamic combinatorial species by solid-state NMR at the atomic level**

DETA was appended to solid-state networks by hydrogen bonds to provide a noncovalent anchoring site for CO_2 (vide supra). Compared to liquid DETA, the structure of DETA-appended MNNs has a rigid and porous nature, resulting in a complex milieu of CO_2
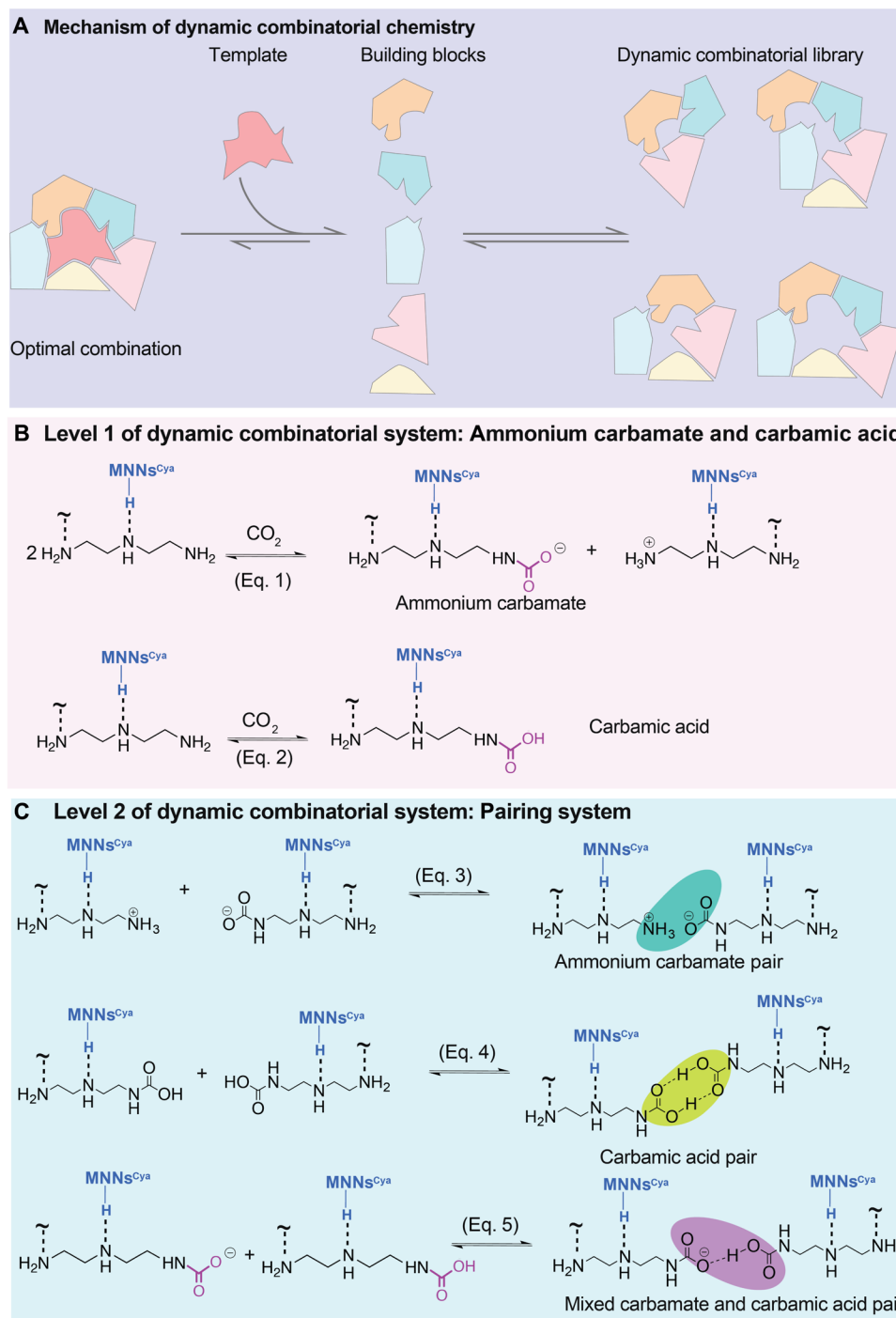
Fig. 3. Five hypothetical CO₂ chemisorption mechanisms in MNNs^{Cya} ⊃ DETA using a double-level dynamic combinatorial system. (**A**) Schematic representation of the fundamental mechanism of DCC. (**B**) Level 1: the reversible carbamate N—CO₂ reactions form ammonium carbamate and carbamic acid (eqs. 1 and 2). (**C**) Level 2: further pairing formation. Bridge formation between oppositely charged (NH₃⁺ and COO⁻) species produces ammonium carbamate pairs (eq. 3). Two carbamic acid species can readily form carbamic acid pairs (eq. 4). The mixed ammonium carbamate and carbamic acid adducts give rise to a hydrogen-bonded structure (eq. 5, charge compensating ammonium group not shown on either side of this equation). H is not shown in eq. 5.

reactions and allowing for the potential formation of monocarbamates and dicarbamates (Fig. 4A). A simplified network of dynamic combinatorial species, where protonation is only partially expressed, is shown in Fig. 4A. Specifically, this process consists of two dynamic combinatorial levels. We start from two pristine structures of MNNs^{Cya} ⊃ DETA, which are denoted d0. With low CO₂ loading, N—CO₂ covalent bonds are generated by the CO₂ addition reactions to the lone pair electrons of the nitrogen, producing protons that

Fig. 4. Demonstration of the dynamic combinatorial species in MNNs^Cya ⊃ DETA by solid-state NMR. (**A**) Depiction of the network of reversible carbamate N—CO_2 reaction sites. (**B**) ^{15}N CP-MAS NMR spectra of MNNs^Cya ⊃ DETA with and without CO_2 adsorption. (**C**) ^1H-^{13}C HETCOR NMR spectrum, with the assignment of observed correlations, for MNNs^Cya ⊃ DETA loaded with CO_2 at 1 bar. The contact time was 100 μs. (**D**) The two-level dynamic combinatorial system of CO_2 chemisorption species as confirmed by NMR. First-level species: ammonium carbamate and carbamic acid. Second-level species: ammonium carbamate/carbamic acid pairs.

generate neighboring ammonium ions. There are two types of amine sites that CO_2 molecules might occupy: primary amine (d1a) and secondary amine (d1s), which form via the reversible reactions, eqs. 6 and 7, respectively (Fig. 4A). In our nomenclature for adducts generated in the dynamic combinatorial systems, s and a denote symmetric and asymmetric carbamate patterns on the networks, respectively. With an excess of CO_2, both primary amines might react with CO_2 molecules, denoted d2s.

Solid-state NMR methods specify the populations within the dynamic combinatorial networks. In particular, natural abundance ^{15}N CP-MAS NMR spectra corroborate CO_2 reaction sites (Fig. 4B and fig. S8). For both MNNs^Cya ⊃ DETA-CO_2 and MNNs ⊃ DETA-CO_2, we observe that the resonances at 20.1 ppm, assignable to nitrogen from primary amines (marked with purple circles), disappeared after loading CO_2 at ~1 bar. This result indicates a conformational carbamate species generated through a primary amine N—CO_2 reaction, in turn implying that CO_2 molecules favor interaction with primary amine nitrogens. This result is also consistent with an analogous

the study in a diamine-appended MOF (22). Furthermore, the peak at 30.3 ppm arising from secondary amine nitrogen remains in the spectrum regardless of CO_2 loading, allowing us to conclude that the secondary amine nitrogens have not reacted with CO_2. In contrast, in the liquid DETA-CO_2 system, CO_2 readily reacts with secondary amines and forms carbamate (8). We theorize that hydrogen bonding interactions between the secondary amine nitrogen (DETA) and MNNs' backbone occupies the lone pair of the secondary amine nitrogen, effectively preventing reaction with CO_2. Correspondingly, we can exclude eq. 7 in our dynamic combinatorial system (Fig. 4A).

To monitor the further reaction of additional CO_2 at high CO_2 loadings, we calculate the mole fraction of chemisorbed CO_2 (mole) for each DETA (mole) in the network. On the basis of the prior structure of DETA-appended MNNs determined via DFT calculations and NMR lineshape analysis, we identify a stoichiometry of 1 CO_2 captured per 1 DETA (table S1). These quantitative calculations reveal that no additional CO_2 molecules react with both primary

amine nitrogen sites (d2s). Thus, we can exclude the reaction shown in eq. 8 and its corresponding adducts (Fig. 4A, d2s). Furthermore, the ^{13}C solid-state NMR spectrum (Fig. 2C) exhibits two resolved peaks (164.7 and 161.1 ppm) in this chemisorbed region, corresponding to ammonium carbamate (dominant) and carbamic acid. The ^{15}N resonance discernible at 84.4 ppm for either MNNs[Cya] ⊃ DETA-CO_2 or MNNs ⊃ DETA-CO_2 is attributed to ammonium carbamate and carbamic acid (22).

To further elucidate the second level (ion-pairing interactions) of the dynamic combinatorial system (Fig. 3C), we perform additional 2D [1]H-^{13}C HETCOR experiments (fig. S9) on MNNs[Cya] ⊃ DETA-CO_2 at 1013 mbar (Fig. 4C). This experiment relies on through-space dipole-dipole interactions to selectively detect [1]H-^{13}C correlations resulting from spatial proximity. A short contact time (100 μs) enables the detection of only those hydrogen atoms closest to the ^{13}C nuclei of the ion-paired species. The HETCOR spectra reveal a dominant correlation at 164.7 ppm and a minor correlation at 161.1 ppm in the ^{13}C dimension, corresponding to ammonium carbamate and carbamic acid, respectively (18). For this dominant ^{13}C resonance at 164.7 ppm, we assign the correlations to the ^{1}H peak of the secondary amine N**H**COO[−] with a chemical shift of 6.1 ppm (Fig. 4C, peak labeled A). A weaker correlation to the 11.2 ppm ^{1}H chemical shift is associated with protons from ammonium carbamate, RN**H**$_3^+$ (Fig. 4C, peak labeled B). As a result, we can see the second-level dynamic combinatorial species (Fig. 3C, eq. 3) in the form of the dominant ion pairing between ammonium and the oxygen atom of the carbamate (Fig. 4D). This conformation is unique among the amine-appended polymer networks, and its formation is likely due to the irregular self-folding of amorphous polymer networks.

The carbamic acid species associated with the ^{13}C resonance at 161.1 ppm present an intense cross-peak (5.5 ppm, peak C) and two less-intense ^{1}H correlations (8.5 ppm, peak D; 12.5 ppm, peak E; Fig. 4C). On the basis of our previous hypothesis, these species could be carbamic acid pairs or mixed carbamate and carbamic acid pairs (Fig. 3C, eqs. 4 and 5). The presence of peak C, however, leads us to conclude that some ammonium ions are strongly correlated to the reacted [13]CO_2, consistent only with eq. 5—the mixed carbamate/carbamic acid pairs. The intensities of the cross-peaks A and C suggest similar [1]H-^{13}C correlations for both moieties, implying that the peaks at 5.5 and 8.5 ppm correspond to protons of N**H**COOH (acid) and RN**H**$_3^+$ (carbamate), respectively. These two major (peaks A and C) and minor (peaks B and D) correlations at these short contact times are anticipated for the mixed carbamic acid/carbamate pair via hydrogen bonds, forming important components of the second level of the DCC system (Fig. 3C, eq. 5), with the relatively short C⋯H distances predicted from DFT calculations (Fig. 5F; 1.95 Å for C⋯H$_{NH_3^+}$ and 2.01 Å for C⋯H$_{NHRCOOH}$). Last, a weak proton signal at 12.5 ppm is tentatively assigned to the acid proton NHRCOO**H** owing to the extreme chemical shift associated with strong O—H hydrogen bonds. Together, the NMR data paint a picture of ion-pairing and hydrogen-bonding interactions that promote the stabilization of the CO_2-inserted phase.

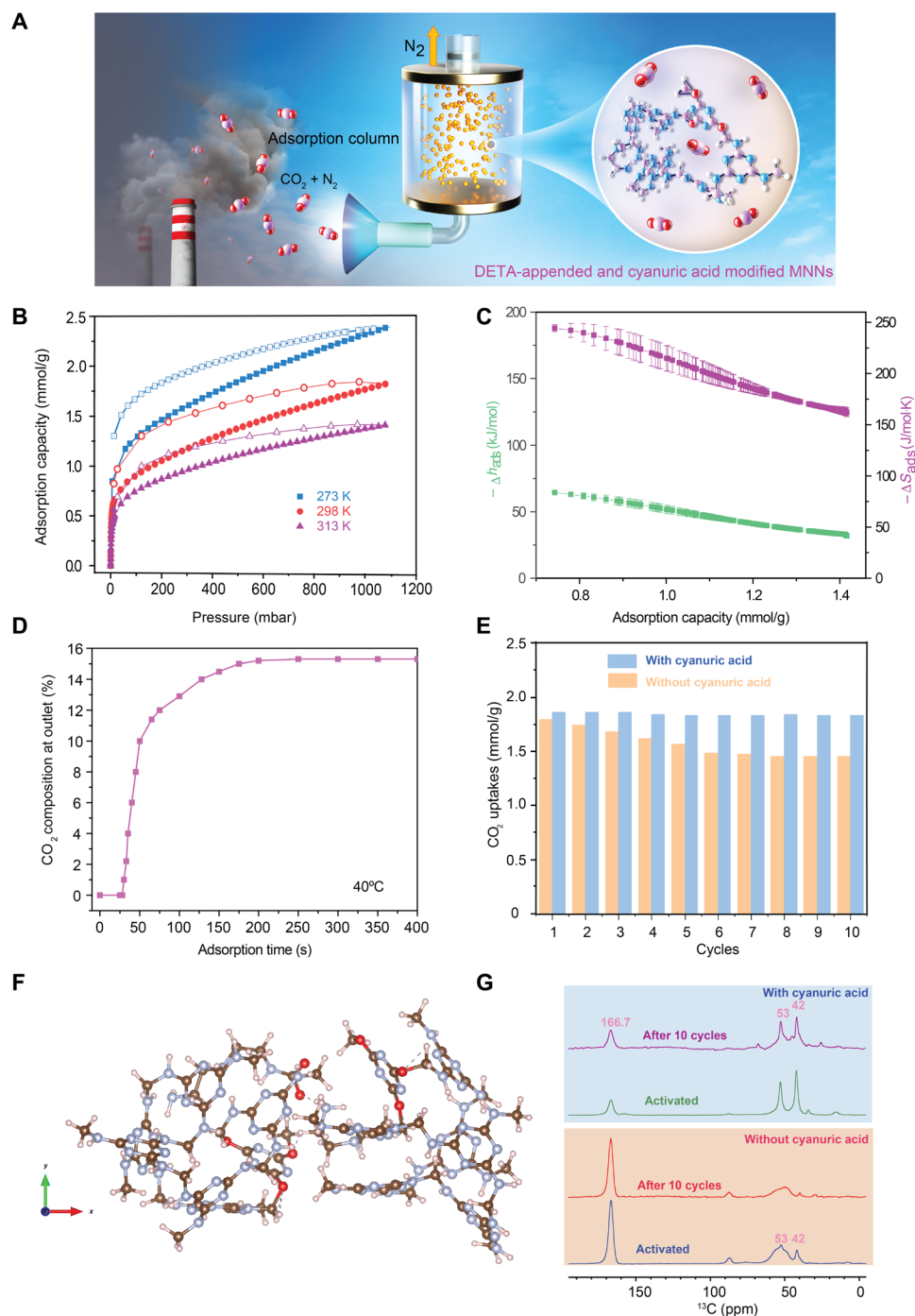## Kinetics of CO_2 adsorption and adsorption-desorption cycles
To better assess the applicability of MNNs[Cya] ⊃ DETA for carbon capture applications, we measured breakthrough curves, cycling stability, and the thermodynamic parameters associated with CO_2 adsorption on this system (28). These measurements follow from

concern about the uncertainties in the recycling time, the lifespan of an adsorbent, and the energy needed to regenerate an adsorbent. DOE's goal for the 90% capture of the CO_2 from natural gas flue stream (~4% CO_2) prompted the CO_2 adsorption and desorption isotherms for MNNs[Cya] ⊃ DETA at 273, 298, and 313 K (Fig. 5, A and B), where we find that 90% CO_2 adsorption efficiency (e.g., removal from 40 to 4 mbar at atmosphere pressure) is easily achieved. Using the Clausius-Clapeyron equation, we calculate differential adsorption enthalpy (Δh_{ads}) and entropy (Δs_{ads}) values of 53 kJ/mol and 217 J/mol·K, respectively, at a CO_2 uptake of 1 mmol of CO_2/g (Fig. 5C). The Δs_{ads} value is roughly analogous to that of MOF-274 (5), as expected because the organization of the carbamate products is roughly equivalent in both sets of materials. The Δh_{ads} (53 kJ/mol) is considerably lower than that of amine-appended MOF-274 (5). These observations suggest that the networks would exhibit lower regeneration energy than amine-functionalized MOFs. The changes in Δh_{ads} with adsorption capacity (Fig. 5C) suggest that CO_2 adsorption sites interact with each other as capacity is increased.

Breakthrough measurements also provide estimates for the time required to cycle adsorption onto MNNs[Cya] ⊃ DETA. Here, we perform adsorption breakthrough experiments with simulated coal-fired power plant flue gas (15% CO_2, 83% N_2, and 2% H_2O) at 313 K (Fig. 5D). Under these conditions, the networks exhibited a high CO_2 capture rate of 90% with a breakthrough capacity of 1.8 mmol/g. These results illustrate that amine-appended network materials not only have low energy consumption for CO_2 but also may exhibit cycling times that can be matched to industrial process equipment.

Last, to investigate the stability of the amine-appended network in the presence of gases during multiple CO_2 adsorption-desorption cycles, CO_2 isotherms were measured at 298 K for 10 adsorption-desorption cycles to reveal the effects of cyanuric acid modification on CO_2 adsorption performance. Figure 5E shows the recorded CO_2 uptakes of MNNs[Cya] ⊃ DETA and MNNs ⊃ DETA over 10 cycles. After 10 cycles, we observe a substantial decrease from 99 to 78% CO_2 capacity at 1 atm for the MNNs ⊃ DETA, yet the CO_2 capacities for the MNNs[Cya] ⊃ DETA sample did not change significantly. We hypothesized that the DETA of MNNs ⊃ DETA sample loses amine functionality over the adsorption-desorption cycles and tested this hypothesis by conducting ^{13}C MAS NMR experiments before and after 10 CO_2 adsorption-desorption cycles. The ^{13}C NMR spectra of MNNs ⊃ DETA following the CO_2 adsorption-desorption cycles are shown in Fig. 5G (marked in orange), while MNNs[Cya] ⊃ DETA is shown in Fig. 5G (marked in blue). In the absence of cyanuric acid, the network DETA peaks at 53 and 42 ppm diminish, suggesting that DETA loading decreases after 10 cycles. We surmise that in the adsorption-desorption process, hydrogen bonds break as CO_2 is inserted, significantly hindering subsequent adsorption performance upon cycling. Unexpectedly, we noted that the two DETA resonances in the spectrum of MNNs[Cya] ⊃ DETA remain unchanged after 10 cycles, from which we conclude that cyanuric acid aids in tethering the DETA molecules to the networks. N—H⋯O hydrogen bonds between cyanuric acid and networks are formed, providing additional stability. The electronegativity of oxygen in N—H⋯O is higher than that of nitrogen in N—H⋯N, and we surmise that this results in greater stabilization of DETA by the cyanuric acid groups. These data illustrate that cyanuric acid– and amine-appended networks, for which the CO_2 chemisorption byproducts can be designed and synthesized via DCC, have extensive and stable CO_2 capture capacities at atmospheric pressures.

Fig. 5. DFT-calculated structures, kinetics of adsorption, and stability of MNNs^Cya ⊃ DETA during CO₂ cycles. (**A**) Schematic diagram of adsorption column system. (**B**) Adsorption (filled shapes) and desorption (open shapes) isotherms for CO_2 uptake in MNNs^Cya ⊃ DETA at 273, 298, and 313 K. (**C**) The $-\Delta h_{ads}$ (enthalpy) and $-\Delta s_{ads}$ (entropy) for MNNs^Cya ⊃ DETA determined using the Clausius-Clapeyron equation as a function of CO_2 loading. (**D**) Adsorption breakthrough and rate for adsorption column of MNNs^Cya ⊃ DETA at 313 K (15% CO_2, 83% N_2, and 2% H_2O). (**E**) Recorded CO_2 uptakes during 10 adsorption-desorption cycles using the homemade dosing setup. (**F**) Proposed mixed chemisorption structure with ammonium carbamate pair. The structure was obtained by DFT modeling at the TPSS-D3(BJ)/6-31G* level. (**G**) ^{13}C NMR (16.4 T) spectra acquired by CP for MNNs ⊃ DETA and MNNs^Cya ⊃ DETA, before and after 10 CO_2 adsorption-desorption cycles.

DISCUSSION

We have synthesized an amine-appended melamine porous network at a kilogram scale that acts as a CO_2 capture material with efficient adsorption, extraordinary cycling stability, and low regeneration energy.

From a dynamic combinatorial framework, we reveal the chemisorption within this porous network as a series of interconnected reactions, elucidated by solid-state ^{13}C and ^{15}N NMR spectroscopy at the atomic level. We have demonstrated a double-level DCC system that includes

reversible carbamate N—CO_2 reactions and interlocked formation of ion pairs. In the first level, we identify the formation of two chemisorbed species consisting of ammonium carbamate (dominant) and carbamic acid (minor), quantified via direct detection ^{13}C NMR spectra. The 2D ^1H-^{13}C HETCOR NMR measurements reveal the second-level dynamic combinatorial species comprising ammonium carbamate pairs and mixed carbamate and carbamic acid pairs. Through quantitative ^{13}C NMR, we determine the local atomic structure of amine-appended MNNs with cyanuric acid, which were confirmed with DFT calculations, and we discerned the equimolar reaction of chemisorbed CO_2 with each DETA molecule. This structure shows conformational carbamate species derived from the reaction of CO_2 with primary amine functionalities. In particular, our results highlight the importance of cyanuric acid modification to enhance the CO_2 chemisorption cycling stability of MNNs-based materials. Solid-state NMR spectroscopy as a nondestructive and atomic-level tool is proven to be an effective way to supplement standard laboratory methods for atomic structure determination in the sustainable energy field. Industrialization of CO_2 capture using networks (e.g., polymers, covalent organic frameworks (COFs), and MOFs) is made possible by this work, which uses atomic-level and DCC design methodologies with accurate mechanism analyses. Integrating scalable nanoporous materials synthesis, chemical engineering, and advanced characterization techniques will accelerate our world's transition to a negative carbon emissions pathway.

MATERIALS AND METHODS

Synthesis of melamine porous network series

Commercially available melamine and paraformaldehyde (Sigma-Aldrich) were used as the starting materials. The scaffold was synthesized through a condensation polymerization at 150° to 170°C in dimethyl sulfoxide (DMSO) for 3 to 7 days (fig. S10) (29). During the polymerization reaction of MNNs, cyanuric acid (7.5 mol %) was mixed with the hot melamine solution (with DMSO as solvent) before the addition of formaldehyde to tether DETA (denoted as MNNs^{Cya}). DETA was mixed with MNNs/MNNs^{Cya} (with hexane as solvent) (denoted as MNNs ⊃ DETA/MNNs^{Cya} ⊃ DETA). The DETA was mixed with MNNs/MNNs^{Cya} in a sonication bath at 50°C for 3 hours. Afterward, the mixture was filtered and washed using tetrahydrofuran, a polar solvent, to remove the residual surface DETA. The collected solid was activated under a vacuum oven at 85°C for 1 hour. All samples were stored in an Ar-filled glovebox for future use.

NMR sample preparation

The activated sample was packed into 4- or 3.2-mm rotors inside an Ar-filled glovebox. At room temperature, $^{13}CO_2$ gas dosing was performed in a custom-built setup shown in fig. S6, featuring an evacuated system in which rotors can be closed with caps using a moveable plunger with an O ring. Gas dosing was carried out at various pressures (10 to 1000 mbar) via a capacitance manometer (model 722B, MKS Instruments). Before gas dosing, the rotor containing the sample was evacuated for at least 10 min inside the glass tube of the custom-built setup. VCR (Swagelok) metal gasket with face seal fittings enabled a metal-to-metal seal, providing a leak-tight system over a pressure range from vacuum to positive pressure. $^{13}CO_2$ gas (99 atomic % of ^{13}C; Sigma-Aldrich) was dosed into the rotor overnight to ensure saturation of the sample. Once equilibrium was reached, the pressure at this condition was recorded and related to $^{13}CO_2$ adsorption capacity.

NMR measurement

All 1D NMR experiments were performed at 500.12 MHz for ^1H (11.7 T) on a Bruker Advance spectrometer with a Bruker narrow bore H/C/N MAS probe (fig. S9A). The ^{13}C/^{15}N MAS NMR spectra were acquired using CP from ^1H to ^{13}C/^{15}N nuclei with heteronuclear decoupling at a sample spinning rate of 10 kHz (fig. S9B). All CP experiments were conducted at a recycle delay of 2 s with a radio frequency field strength of ~25 to 70 kHz, with a contact time of 2 ms. The quantitative ^{13}C direct excitation experiments were carried out with heteronuclear decoupling during detection and sufficiently long recycle delays, 200 s, allowing the nuclei to fully relax between scans. The 2D ^1H-^{13}C HETCOR experiments were conducted at 16.4 T (700 MHz for ^1H) using a Bruker 3.2-mm MAS probe at a spinning rate of 15 kHz with a radio frequency field strength of ~80 kHz. The CP (^1H to ^{13}C) pulse sequence was 90° (^1H) – t_1 – CP – t_2, with a contact time of 100 μs. A ^1H 90° one-pulse sequence was used for ^1H NMR experiments. ^1H, ^{13}C, and ^{15}N chemical shifts were calibrated using ^{13}C-labeled adamantane and ^{15}N-labeled glycine, referenced to 1.85 ppm (adamantane; ^1H), 38.5 ppm (adamantane, tertiary carbon; ^{13}C), and 33.4 ppm (glycine; ^{15}N), respectively.

DFT calculations

To determine the DETA and cyanuric acid–modified MNN structure along with CO_2-adsorbed local structure, DFT calculations were carried out on the Massachusetts Green High Performance Computing Center (30, 31), using the Q-Chem 5.4 package. The cluster structures of CO_2, DETA, MNNs, MNNs ⊃ DETA, MNNs ⊃ DETA-CO_2, MNNs^{Cya} ⊃ DETA, and MNNs^{Cya} ⊃ DETA-CO_2 were optimized at the TPSS-D3(BJ)6-31G* level (Fig. 5F and figs. S14 to S21).

CO_2 adsorption isotherms and breakthrough measurement

The CO_2 adsorption isotherms were measured gravimetrically using a sorption analyzer (model VTI-SA, TA Instruments) at 298 K with CO_2 as the carrier gas. Samples were first degassed at 85°C under a vacuum for 1 hour. The evacuated tube recorded the equilibrium weight of the degassed sample in response to a step change in the concentration of the CO_2 (relative pressure range of 0.01 to 1). Approximately 80 to 90 mg of sample was weighed and placed into the tube of the analyzer. Equilibrium was defined to be reached when the weight changed by less than 0.001% over an interval of 30 s.

A custom-built setup for breakthrough measurement, shown schematically in Fig. 5A, was used to perform breakthrough adsorption measurements. N_2 was used as the carrier gas. During the adsorption process, the mixed N_2 and CO_2 were obtained from Airgas Inc. The mass flow controller (I-Series IP66, MFC) was used to precisely control the flow rate. The effluent gas concentration was measured via a capacitance manometer (model 722B, MKS Instruments). The outlet concentration was recorded every minute until the outlet gas concentration was stabilized at 99% of the inlet concentration.

REFERENCES AND NOTES

1. R. F. Service, Carbon capture marches toward practical use. *Science* **371**, 1300 (2021).
2. L. Rosa, J. A. Reimer, M. S. Went, P. D'Odorico, Hydrological limits to carbon capture and storage. *Nat. Sustain.* **3**, 658–666 (2020).

3. S. Mallapaty, How China could be carbon neutral by mid-century. *Nature* **586**, 482–483 (2020).

4. U.S. Environmental Protection Agency, "Inventory of U.S. Greenhouse Gas Emissions and Sinks: 1990–2018" (Publication 430-R-20-002, U.S. Environmental Protection Agency, 2020); https://epa.gov/sites/default/files/2020-04/documents/us-ghg-inventory-2020-main-text.pdf.

5. E. J. Kim, R. L. Siegelman, H. Z. H. Jiang, A. C. Forse, J.-H. Lee, J. D. Martell, P. J. Milner, J. M. Falkowski, J. B. Neaton, J. A. Reimer, S. C. Weston, J. R. Long, Cooperative carbon capture and steam regeneration with tetraamine-appended metal-organic frameworks. *Science* **369**, 392–396 (2020).

6. A. Zoelle, D. Keairns, L. L. Pinkerton, M. J. Turner, M. Woods, N. Kuehn, V. Shah, V. Chou, "Cost and performance baseline for fossil energy plants volume 1a: Bituminous coal (PC) and natural gas to electricity revision 3" (Technical Report DOE/NETL-2015/1723, National Energy Technology Laboratory, U.S. Department of Energy, 2015).

7. P. G. Boyd, A. Chidambaram, E. García-díez, C. P. Ireland, T. D. Daff, R. Bounds, A. Gładysiak, P. Schouwink, S. M. Moosavi, M. M. Maroto-valer, J. A. Reimer, J. A. R. Navarro, T. K. Woo, S. Garcia, K. C. Stylianou, B. Smit, Data-driven design of metal–Organic frameworks for wet flue gas CO_2 capture. *Nature* **576**, 253–256 (2019).

8. J. Septavaux, C. Tosi, P. Jame, C. Nervi, R. Gobetto, J. Leclaire, Simultaneous CO_2 capture and metal purification from waste streams using triple-level dynamic combinatorial chemistry. *Nat. Chem.* **12**, 202–212 (2020).

9. G. Lee, Y. C. Li, J. Y. Kim, T. Peng, D. H. Nam, A. Sedighian Rasouli, F. Li, M. Luo, A. H. Ip, Y. C. Joo, E. H. Sargent, Electrochemical upgrade of CO_2 from amine capture solution. *Nat. Energy* **6**, 46–53 (2021).

10. H. Furukawa, K. E. Cordova, M. O'Keeffe, O. M. Yaghi, The chemistry and applications of metal-organic frameworks. *Science* **341**, 1230444 (2013).

11. B. Ghalei, K. Sakurai, Y. Kinoshita, K. Wakimoto, A. P. Isfahani, Q. Song, K. Doitomi, S. Furukawa, H. Hirao, H. Kusuda, S. Kitagawa, E. Sivaniah, Enhanced selectivity in mixed matrix membranes for CO_2 capture through efficient dispersion of amine-functionalized MOF nanoparticles. *Nat. Energy* **2**, 1–9 (2017).

12. T. Li, Y. Zhai, S. He, W. Gan, Z. Wei, M. Heidarinejad, D. Dalgo, R. Mi, X. Zhao, J. Song, J. Dai, C. Chen, A. Aili, A. Vellore, A. Martini, R. Yang, J. Srebric, X. Yin, L. Hu, A radiative cooling structural material. *Science* **364**, 760–763 (2019).

13. B. Reif, S. E. Ashbrook, L. Emsley, M. Hong, Solid-state NMR spectroscopy. *Nat. Rev. Methods Prim.* **1**, 2 (2021).

14. X. Kong, H. Deng, F. Yan, J. Kim, J. A. Swisher, B. Smit, O. M. Yaghi, J. A. Reimer, Mapping of functional groups in metal-organic frameworks. *Science* **341**, 882–885 (2013).

15. Z. Jiang, X. Xu, Y. Ma, H. S. Cho, D. Ding, C. Wang, J. Wu, P. Oleynikov, M. Jia, J. Cheng, Y. Zhou, O. Terasaki, T. Peng, L. Zan, H. Deng, Filling metal–Organic framework mesopores with TiO_2 for CO_2 photoreduction. *Nature* **586**, 549–554 (2020).

16. R. T. S. Lam, A. Belenguer, S. L. Roberts, C. Naumann, T. Jarrosson, S. Otto, J. K. M. Sanders, Amplification of acetylcholine-binding catenanes from dynamic combinatorial libraries. *Science* **308**, 667–669 (2005).

17. D. Zhao, J. Feng, Q. Huo, N. Melosh, G. H. Fredrickson, B. F. Chmelka, G. D. Stucky, Triblock copolymer syntheses of mesoporous silica with periodic 50 to 300 angstrom pores. *Science* **279**, 548–552 (1998).

18. M. C. B. G. Nilo, T. G. Simões, C. C. Neto, Using bar infrared spectra and coincidence indexes to study the diversity of solid cyanuric acid structures. *J. Braz. Chem. Soc.* **29**, 1499–1515 (2018).

19. H. Mao, J. Tang, J. Xu, Y. Peng, J. Chen, B. Wu, Y. Jiang, K. Hou, S. Chen, J. Wang, H. R. Lee, D. M. Halat, B. Zhang, W. Chen, A. Z. Plantz, Z. Lu, Y. Cui, J. A. Reimer, Revealing molecular mechanisms in hierarchical nanoporous carbon via nuclear magnetic resonance. *Matter* **3**, 2093–2107 (2020).

20. J. Tao, J. P. Perdew, V. N. Staroverov, G. E. Scuseria, Climbing the density functional ladder: Nonempirical meta–generalized gradient approximation designed for molecules and solids. *Phys. Rev. Lett.* **91**, 146401 (2003).

21. T. M. McDonald, J. A. Mason, X. Kong, E. D. Bloch, D. Gygi, A. Dani, V. Crocellà, F. Giordanino, S. O. Odoh, W. S. Drisdell, B. Vlaisavljevich, A. L. Dzubak, R. Poloni, S. K. Schnell, N. Planas, K. Lee, T. Pascal, L. F. Wan, D. Prendergast, J. B. Neaton, B. Smit, J. B. Kortright, L. Gagliardi, S. Bordiga, J. A. Reimer, J. R. Long, Cooperative insertion of CO_2 in diamine-appended metal-organic frameworks. *Nature* **519**, 303–308 (2015).

22. A. C. Forse, P. J. Milner, J. H. Lee, H. N. Redfearn, J. Oktawiec, R. L. Siegelman, J. D. Martell, B. Dinakar, L. B. Porter-Zasada, M. I. Gonzalez, J. B. Neaton, J. R. Long, J. A. Reimer, Elucidating CO_2 chemisorption in diamine-appended metal-organic frameworks. *J. Am. Chem. Soc.* **140**, 18016–18031 (2018).

23. J. Li, P. Nowak, S. Otto, Dynamic combinatorial libraries: From exploring molecular recognition to systems chemistry. *J. Am. Chem. Soc.* **135**, 9222–9239 (2013).

24. C. G. Pappas, R. Shafi, I. R. Sasselli, H. Siccardi, T. Wang, V. Narang, R. Abzalimov, N. Wijerathne, R. V. Ulijn, Dynamic peptide libraries for the discovery of supramolecular nanomaterials. *Nat. Nanotechnol.* **11**, 960–967 (2016).

25. V. Y. Mao, P. J. Milner, J. H. Lee, A. C. Forse, E. J. Kim, R. L. Siegelman, C. M. McGuirk, L. B. Porter-Zasada, J. B. Neaton, J. A. Reimer, J. R. Long, Cooperative carbon dioxide adsorption in alcoholamine- and alkoxyalkylamine-functionalized metal–Organic frameworks. *Angew. Chem. Int. Ed.* **59**, 19468–19477 (2020).

26. J. Leclaire, L. Vial, S. Otto, J. K. M. Sanders, Expanding diversity in dynamic combinatorial libraries: Simultaneous exchange of disulfide and thioester linkages. *Chem. Commun.* **15**, 1959–1961 (2005).

27. C. H. Chen, D. Shimon, J. J. Lee, F. Mentink-Vigier, I. Hung, C. Sievers, C. W. Jones, S. E. Hayes, The "missing" bicarbonate in CO_2 chemisorption reactions on solid amine sorbents. *J. Am. Chem. Soc.* **140**, 8648–8651 (2018).

28. R. Sathre, E. Masanet, Prospective life-cycle modeling of a carbon capture and storage system using metal-organic frameworks for CO_2 capture. *RSC Adv.* **3**, 4964–4975 (2013).

29. G. S. Day, H. F. Drake, E. A. Joseph, M. Bosch, K. Tan, J. A. Willman, V. Carretier, Z. Perry, W. Burtner, S. Banerjee, O. K. Ozdemir, H. C. Zhou, Improving alkylamine incorporation in porous polymer networks through dopant incorporation. *Adv. Sustainable Syst.* **3**, 1–7 (2019).

30. K. Wolinski, J. F. Hinton, P. Pulay, Efficient implementation of the gauge-independent atomic orbital method for NMR chemical shift calculations. *J. Am. Chem. Soc.* **112**, 8251–8260 (1990).

31. J. J. Olivero, R. L. Longbothum, Empirical fits to the voigt line width: A brief review. *J. Quant. Spectrosc. Radiat. Transf.* **17**, 233–236 (1977).